RSC Advances

PAPER

View Article Online
View Journal | View Issue

Cite this: *RSC Adv.*, 2026, **16**, 14936

Expired chlorzoxazone/*N*-acetyl-*para*-aminophenol as corrosion inhibitor for 304 stainless steel in hydrochloric acid

Hani Nassser Abdelhamid *[a] and Mohamed E. Eissa [b]

The influence of the expired drug chlorzoxazone (*N*-acetyl-*para*-aminophenol) on the corrosion behavior of 304 stainless steel (304SS) in 1.0 M hydrochloric acid was examined. Several electrochemical measurements were investigated, including open circuit potential (OCP), cyclic voltammetry (CV), potentiodynamic polarization (PD), electrochemical potentiokinetic reactivation (EPR), chronopotentiometry (CP), chronoamperometry (CA), linear sweep voltammetry (LSV), and electrochemical impedance spectroscopy (EIS) using Nquist and Bode plots. These methods were analyzed to evaluate the corrosion rate, passivation characteristics, and stability of protective films with different drug concentrations (50–400 ppm). Open-circuit measurements indicated that the incorporation of the drug altered the potential to more noble levels, suggesting surface protection. CV and LSV measurements revealed a significant reduction in current density with increasing drug concentration, validating the robust adsorption of the inhibitor molecules and establishing a stable passive film. PD and EPR findings indicated substantial decreases in corrosion current density (I_{corr}) and increases in polarization resistance (R_p), especially at 400 ppm, where the corrosion rate was the lowest among different drug loadings. Chronopotentiometry demonstrated consistent potential responses and improved passivation with the inhibitor, whilst chronoamperometry showed a significant reduction in dissolving current relative to uncoated steel. The data collectively indicate that the drug compound functions as an effective, concentration-dependent corrosion inhibitor, establishing a protective barrier that mitigates both anodic and cathodic processes, thus improving the electrochemical stability of stainless steel in acidic environments. This study opens a new avenue for reusing expired drugs as corrosion inhibitors.

Received 6th November 2025
Accepted 6th March 2026

DOI: 10.1039/d5ra08536e

rsc.li/rsc-advances

Introduction

The ductility, strength, and self-passivating chromium oxyhydroxide layer of 304 stainless steel (304SS) make it a popular choice for several industrial applications.[1,2] 304SS is an essential component of nuclear power plant (NPP) cooling systems due to its mechanical robustness, ductility, heat resistance, and corrosion resistance. Nevertheless, the accumulation of surface contaminants, including scale, rust, and pollutants, frequently occurs during extended industrial use, necessitating post-use cleansing. The conventional pickling process, typically conducted in hot hydrochloric acid (65–80 °C), effectively removes scale while simultaneously promoting metal dissolution and corrosion.[3] 304SS stainless steel is a metastable austenitic alloy, with its corrosion resistance predominantly influenced by the stability of the γ-austenite phase and the integrity of the passive Cr_2O_3-rich surface coating. In chloride environments, localized passivation failure can be influenced by factors such as chloride adsorption, local acidification, and mechanical or electrochemical conditions. Consequently, it is imperative to implement effective corrosion mitigation strategies. Several studies have concentrated on integrating surface modification techniques and anticorrosive additives to address this issue. Among these, anodization has become a cost-effective and efficient method for producing nanoporous oxide films that substantially improve the durability, adhesion, and corrosion resistance.[4] Adjusting anodization parameters can produce oxide films with customized thicknesses, morphologies, and constituents. These nanoporous layers are highly regarded for their extensive industrial applicability, scalability, and impurity-free nature in the chemical, oil, construction, transportation, and nuclear sectors. The anti-corrosion characteristics of 304 SS can be achieved *via* anodized and hydrophobic modification.[5] The modification enabled the formation of a well-ordered hexagonally closed-packed nanoporous oxide layer on the 304 SS surface, facilitating high electrochemical anodization and subsequent annealing. The chemical modification also included a self-assembled monolayer of silane molecules, specifically

[a]*Department of Chemistry, Faculty of Science, Assiut University, Assiut, 71515, Egypt*
[b]*Chemistry Department, College of Science, Imam Mohammad Ibn Saud Islamic University (IMSIU), Riyadh 11623, Saudi Arabia. E-mail: hany.abdelhamid@aun.edu.eg*

octadecyltrimethoxysilane (ODTS) and perfluorooctyltriethoxysilane (PFTS). This method offered a corrosion inhibition efficiency of 92.06%.[5] There are other modification methods, including surface modification using stearic acid,[6–8] myristic acid,[9] pentafluoroethane,[10] perfluorooctanesulfonic acid,[11] metal–organic frameworks,[11] or tridecafluoroctyltriethoxysilane.[12] However, these processes are tedious and require several steps.[13] Furthermore, the protective nanoporous oxide layer undergoes corrosive degradation due to the moisture and corrosive vapors or particles contained within it.

Several molecules have been reported as corrosion inhibitors, including plant extracts,[14,15] surfactants,[16,17] polysaccharides,[18] metal oxides,[19–21] and microbial technology,[22] *e.g.*, *Escherichia coli* biofilm.[23] Plant extracts were reported, including *Tithonia diversifolia* (Hemsl) A. grey leaf extract (TDLE),[24] *Melaleuca leaves*,[25] *Ruta graveolens*,[26] *Lavender angustifolia*,[27] *Celastrus paniculatus*,[28] *Nicotiana tabacum*,[29] and *Prunus domestica*.[30] Green solvents such as ionic liquids were also reported.[31] Organic molecules such as Schiff's base,[32] bispyrazole derivative,[33] or phytic acid/sodium phosphate[34] can be used as corrosion inhibitors. Polymers or biopolymers inhibit corrosion, including polymers such as poly(ethylene terephthalate) (PET),[35] *N*-vinylcaprolactam-acrylamide,[36] chitosan,[37] and a composite of different polymers.[38] Drugs can also be used as inhibitors.[39] Synthetic nanomaterials were reported as inhibitors, including a layered double hydroxide[40] and bimetallic organic framework (CuNi-MOF).[41] These materials exhibit low efficiency or are reported in less aggressive media such as 3.5 wt% NaCl.[34,40] Waste materials can be reused for corrosion inhibition, including cattle manure,[42] and expired chloroquine phosphate.[43] Corrosion inhibitors, particularly heterocyclic organic compounds, are among the most effective solutions for safeguarding 304 SS in corrosive media. Their inhibitory effect results from adsorption onto the steel surface, which creates a protective barrier. The efficiency of metal–inhibitor coordination is significantly influenced by molecular features, including heteroatoms (N, O, P, S), aromatic rings, or extended carbon chains.

This study investigates the corrosion behavior of 304SS in 1.0 M HCl in the presence of expired chlorzoxazone/*N*-acetyl-*para*-aminophenol. The inhibition was evaluated using electrochemical measurements of open-circuit potential (OCP), cyclic voltammetry (CV), electrochemical potentiokinetic reactivation (EPR), potentiodynamic (PD), chronopotentiometry (CP), chronoamperometry (CA), linear sweep voltammetry (LSV), electrochemical impedance spectroscopy (EIS), and scanning electron microscopy (SEM) images. The expired drug exhibited effective corrosion inhibition. This study shows that expired drugs can be reused as corrosion inhibitors for stainless steel.

Experimental

Materials and reagents

Stainless steel type 304 was purchased from Chenyaping (Putian City, China). The composition of stainless steel type 304 contains 0.045% C, 0.35% Si, 1.64% Mn, 0.17% Co, 0.026% P, 0.014% S, 18.0% Cr, 8.8% Ni, 0.19% Mo, 0.16% Cu, and 0.044% N. The remaining represents the Fe content in 304SS. Chlorzoxazone and *N*-acetyl-*para*-aminophenol were purchased from a local pharmacy in Riyadh (Saudi Arabia).

Chemicals and solutions

The stock solution of chlorzoxazone and *N*-acetyl-*para*-aminophenol (Fig. 1a) was prepared in distilled water. Stock solutions of 1000 ppm of the examined pharmaceutical compound were prepared by dissolving 1 g L^{-1} of the solid drug in water; subsequent concentrations ranging from 50 to 400 ppm were obtained by dilution with water. All materials utilized were of analytical reagent quality and employed as received. A Na_2SO_4 solution was used as the control electrolyte. It exhibits no signs of corrosion; thus, it can be considered a negative control experiment.

Electrochemical measurements

The 304SS strips, measuring 1 × 2 cm^2, were utilized for all measurements (Fig. 1b). The specimens are soaked in 50 mL of the test solution. Potentiostatic polarization experiments were conducted using the Corrtest CS150M (Corrtest®, Wuhan, China). The electrode potential was measured relative to the Ag/

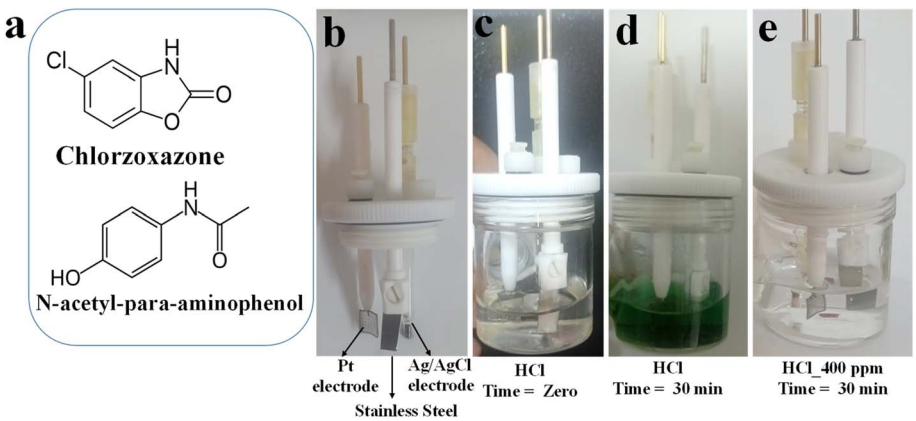

Fig. 1 (a) chemical structure for chlorzoxazone and *N*-acetyl-*para*-aminophenol, (b) cells setup, (c) solution before measurement, (d and e) after measurement for (d) without and (e) with drug.

AgCl reference electrode, with a platinum foil counter electrode. The electrochemical measurements were assessed using OCP, CV, EPR, PD, CP, CA, and LSV. Measurements were repeated 2–3 times. The OCP values reported with a standard deviation of 3 measurements. CV curves were measured at a scan rate of 100 mV s^{-1} with the potential window of −0.4 V to +0.5 V. The PD measurements were performed at an OCP of −0.20233 V, with an electrode area of 1 cm^2, a density of 7.8 g cm^{-3}, and a Stern–Geary constant of 26. The potential was scanned from −0.4 V to +0.5 V *versus* the reference electrode at a scan rate of 3 mV s^{-1} and a frequency of 6 Hz. The resulting polarization curves reveal the influence of drug concentration on both anodic and cathodic reactions. The anodic (β_a) and cathodic (β_c) Tafel slopes were determined by extrapolating the linear regions of the polarization curves, and the polarization resistance (R_p) was calculated using the Stern–Geary equation (eqn (1)).[44] These parameters provide valuable insights into the materials' corrosion inhibition efficiency and electrochemical kinetics under the tested conditions. Data analysis and calculation were computed using CS analysis (Studio 6, Corrtest®). Tafel and Tafel (LEV), a non-linear least-squares algorithm based on the Levenberg–Marquardt Method (LEV) were reported for evaluating corrosion inhibition, computing corrosion current, corrosion potential, and corrosion rate.

$$R_p = \frac{\beta_a \times \beta_c}{2.303 \times i_{Corr}(\beta_a + \beta_c)} \quad (1)$$

The surface coverage (θ, eqn (2)) and corrosion inhibition efficiency (η, eqn (3)) were determined from electrochemical parameters, based on corrosion current density values obtained in the absence and presence of the drug.[45]

$$\theta = \frac{i_{corr,0} - i_{corr}}{i_{corr,0}} \quad (2)$$

$$\eta = \frac{i_{corr,0} - i_{corr}}{i_{corr,0}} \times 100 \quad (3)$$

Electrochemical impedance spectroscopy (EIS) was measured using Nquist and Bode plots with a bipotentiostat CS350M (Corrtest®). Measurements were performed at least two times to ensure reproducibility.

Surface characterization

Surface analysis of 304SS, pristine and after treatment with 50 ppm and 400 ppm of the drug solution, was evaluated using scanning electron microscopy (SEM, Quattro S, Thermo Scientific).

Results and discussion

Corrosion inhibitors and electrochemical setup

Fig. 1 depicts the chemical and experimental configuration employed to examine the corrosion inhibition properties of two medicinal compounds, chlorzoxazone and *N*-acetyl-*para*-aminophenol (acetaminophen), on 304 stainless steel in an acidic environment. Fig. 1a illustrates the molecular structures of both drugs, emphasizing their essential functional groups that contribute to corrosion inhibition. Chlorzoxazone has aromatic and heterocyclic frameworks including amine (–NH), chloride (Cl), and carbonyl (C=O) functionalities, whereas *N*-acetyl-*para*-aminophenol contains hydroxyl (–OH) and amide (–NH–CO–) groups. These functional groups serve as active adsorption centers, donating lone pairs or π-electrons to the unoccupied d-orbitals of iron atoms on the stainless steel surface, forming a protective chemisorbed coating that impedes metal breakdown.

Fig. 1b illustrates the electrochemical cell arrangement, comprising stainless steel as the working electrode, Ag/AgCl as the reference electrode, and platinum as the counter electrode. The solution before measurement appears transparent, highlighting the electrolyte's original state (Fig. 1c). Post-measurement, the cell without drug additives displays a pronounced green color, indicating the formation of $FeCl_2$ and $FeCl_3$, confirming substantial corrosion and dissolution of the stainless steel surface (Fig. 1d). Conversely, the cell containing 400 ppm of chlorzoxazone or *N*-acetyl-*para*-

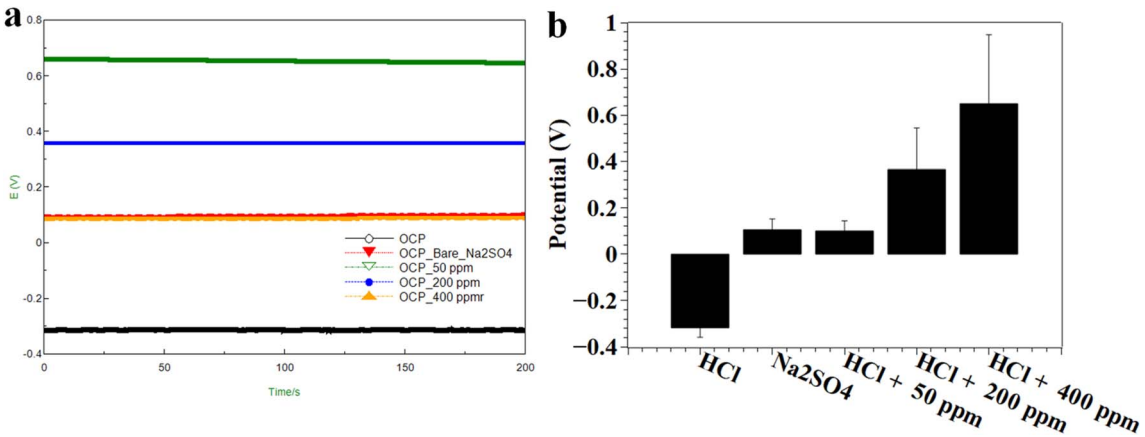

Fig. 2 (a) OCP and (b) onset potential *vs.* condition. Error bars represent standard deviations.

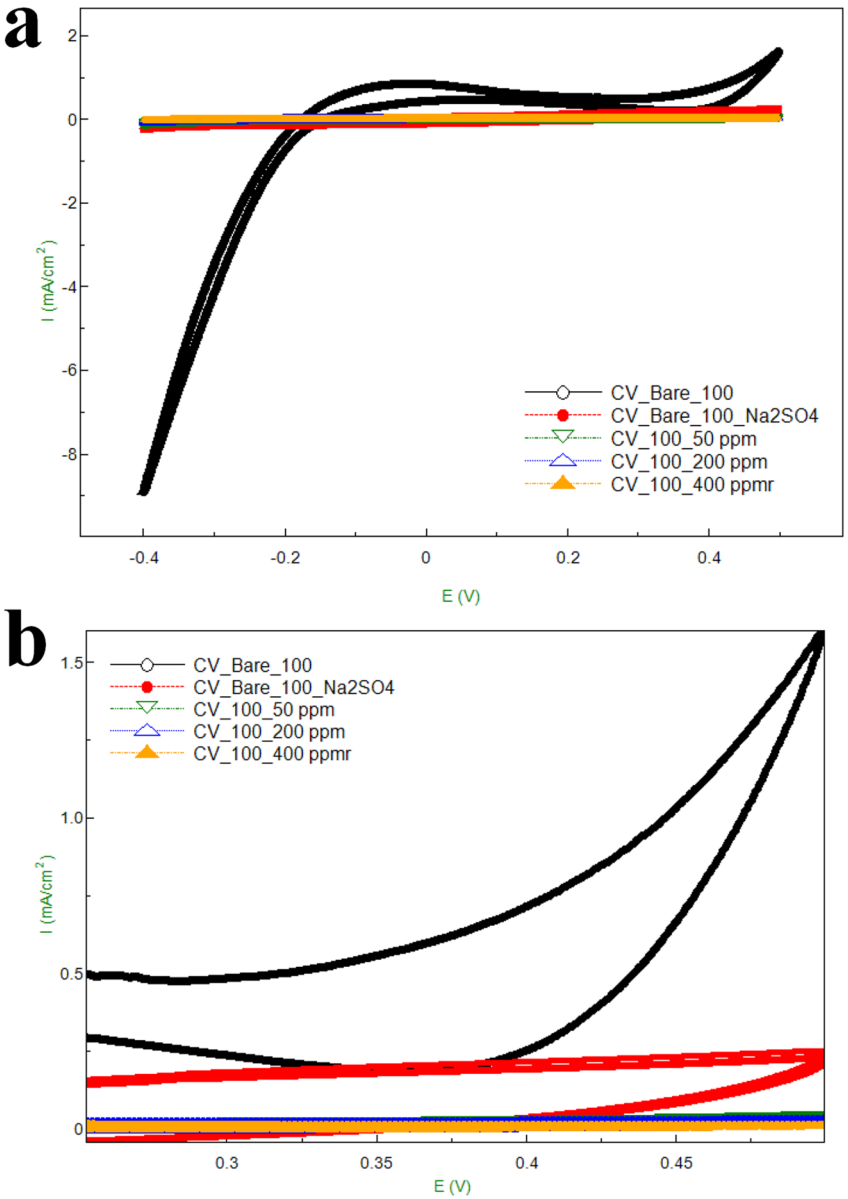

Fig. 3 (a and b) CV curves for (a) whole curve, and (b) enlarged curves.

aminophenol maintains a transparent solution, with the stainless steel electrode visible with no dissolution (Fig. 1e). This observation verifies that drugs efficiently mitigate corrosion by adsorbing onto the metal surface, blocking active sites, and preventing chloride-ion attack. The results unequivocally indicate that including these organic inhibitors significantly enhances the corrosion resistance of stainless steel in acidic environments.

Electrochemical measurements

A comprehensive electrochemical analysis was performed to assess the corrosion characteristics of 304 stainless steel in 1.0 M HCl and Na_2SO_4 solutions with varying concentrations (50, 200, and 400 ppm) of the drug inhibitor. The measurements included OCP (Fig. 2), CV (Fig. 3), PD (Fig. 4a), EPR (Fig. 4b), CP (Fig. 5a)/CA (Fig. 5b), LSV (Fig. 6), SEM images (Fig. 7), and EIS (Fig. 8).

The OCP measurements provided a preliminary assessment of corrosion propensity under each condition (Fig. 2). In 1 M HCl, a significantly negative open circuit potential (−0.318 V) indicated active dissolving and the degradation of the passive layer caused by chloride ion infiltration. Conversely, Na_2SO_4 demonstrated a potential of +0.105 V, indicating the durability of the passive oxide layer. As drug concentration increased, the OCP transitioned to more noble values (+0.1, +0.366, and +0.65 V), indicating that the drug inhibitor efficiently adsorbed onto the metal surface and improved passivation by decreasing the active corrosion rate. The OCP results for 304 SS exhibit a distinct, consistent trend toward noble potentials (all values reported relative to Ag/AgCl) as the medium transitions from an aggressive chloride-containing acid to a sulfate or HCl medium

with increasing drug concentration. The OCP in 1 M HCl is −0.318 V, indicative of active corrosion resulting from chloride-induced degradation of the passive film. Conversely, the electrode in Na_2SO_4 exhibits a positive OCP of +0.105 V, indicating a passive, less reactive surface in this non-chloride electrolyte. Upon adding the drug to HCl, the OCP shifts progressively in the positive direction with increasing concentration: +0.10 V at 50 ppm, +0.366 V at 200 ppm, and +0.65 V at 400 ppm. Two primary conclusions emerge from these tendencies. The substantial negative-to-positive transition between HCl and Na_2SO_4 validates the potent corrosive impact of chloride. The positive shifts in OCP with increasing drug concentration indicate that organic molecules are adsorbing onto the stainless-steel surface, thereby modifying the electrochemical balance towards a more passive state. In practical terms, the adsorption and film formation by the inhibitor obstruct active dissolving sites and/or compete with Cl^- adsorption, rendering the metal surface thermodynamically less susceptible to oxidation; the OCP becomes more noble as inhibitor coverage increases. It is crucial to recognize that OCP serves as a steady-state indication; the constancy of these potentials throughout the measurement indicates a stable surface condition, a consistent adsorbed coating, or a stable corrosion regime. Nevertheless, OCP alone fails to assess inhibitory efficiency or kinetic characteristics. Consequently, these favorable OCP shifts should be analyzed with other electrochemical measurements.

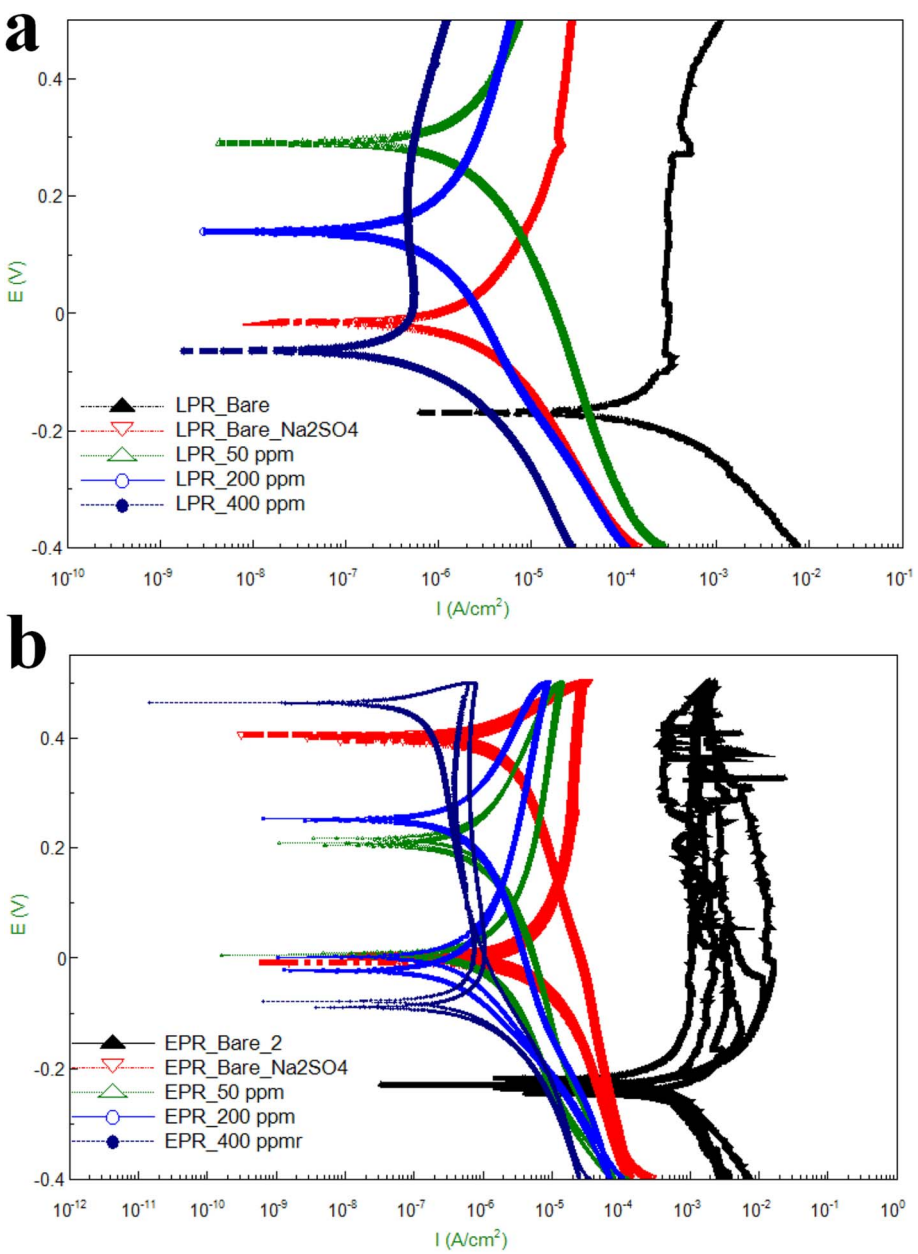

Fig. 4 (a) Potenodynamic (PD) and (b) electrochemical potentiokinetic reactivation (EPR).

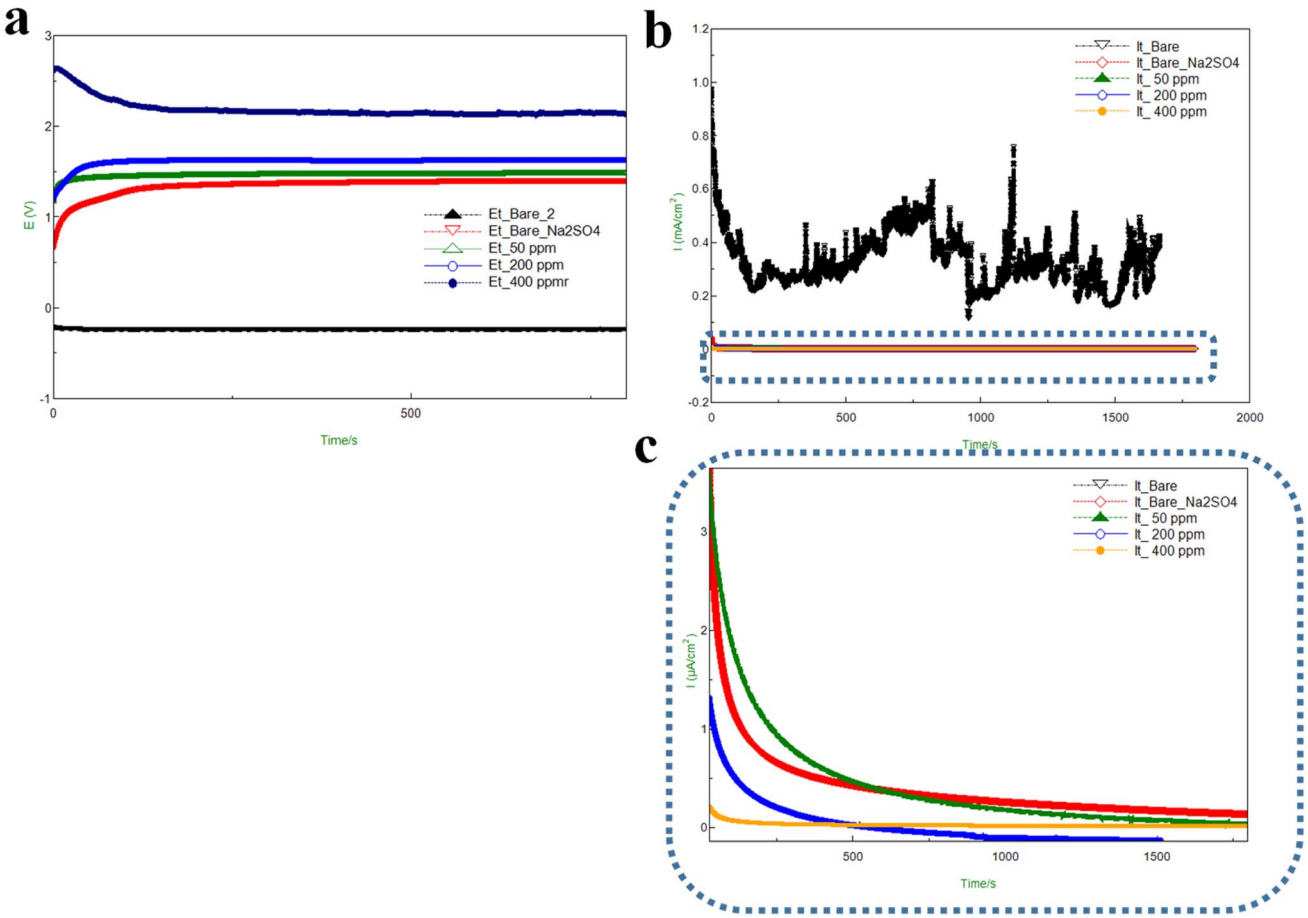

Fig. 5 (a) chronopotentiometry and (b) chronoamperometry and (c) represented enlarged and highlighted regions.

CV analysis was used to investigate the redox behavior and passivation properties of the stainless steel surface (Fig. 3). In HCl, CV demonstrated significant anodic dissolution and hysteresis loops characteristic of localized pitting corrosion. In Na_2SO_4, the CV voltammograms exhibited a more uniform current response, indicating passive behavior. Incorporating the drug markedly decreases both anodic and cathodic current densities and decreases hysteresis, validating its efficacy in inhibiting corrosion and averting pit formation. Fig. 3 presents the CV curves depicting the electrochemical behavior of 304 stainless steel in 1 M HCl, 1 M Na_2SO_4, and 1 M HCl with varying concentrations of the drug inhibitor (50, 200, and 400 ppm).

The current density (I, A cm^{-2}) *versus* potential (E, V) profiles exhibit distinct trends that depend on the medium and inhibitor concentration, providing insights into corrosion and passivation mechanisms (Fig. 3). The stainless steel in HCl shows the highest current density, indicating active dissolution and severe corrosion from chloride-ion attack, which degrades the protective oxide layer and facilitates anodic metal dissolution (Fig. 3). The curve's shape, characterized by steep current rises at high potentials, validates passivity breakdown and localized corrosion initiation, including pitting. Conversely, the Na_2SO_4 medium has a significantly reduced current response, indicating a solid passive coating and less corrosion activity. Sulfate ions are less aggressive than chloride ions, facilitating the formation of a more protective oxide layer on the steel surface. Introducing the drug inhibitor to the HCl solution significantly decreases current density at all concentrations (50–400 ppm). This decrease indicates the adsorption of drug molecules onto the stainless steel surface, creating a protective barrier that hinders charge transfer and inhibits metal dissolution. The gradual decline in current density with increasing inhibitor concentration indicates a dose-dependent inhibitory effect, with 400 ppm providing the most effective corrosion mitigation, resulting in a nearly horizontal CV curve with negligible current fluctuations over the potential range. The CV results substantiate that the medication is an efficacious corrosion inhibitor for stainless steel under acidic conditions. Inhibitory efficiency increases with concentration due to the formation of a dense, adherent film of drug molecules that stabilizes the passive layer and blocks both anodic and cathodic reactions. This trend aligns with the OCP findings, indicating that the potential shifted toward more noble values in the presence of the inhibitor, thereby reinforcing the improved corrosion resistance observed with drug inclusion (Fig. 3).

Fig. 4 illustrates the PD and EPR measurements of 304SS in several corrosive environments: 1 M HCl, Na_2SO_4, and HCl with

differing concentrations (50, 200, and 400 ppm) of the examined medication. These measurements elucidate corrosion kinetics, passivation behavior, and the drug's inhibitory efficiency. The PD curves demonstrate that stainless steel in HCl exhibits a high dissolution region, characterized by a corrosion potential (E_0) of approximately −0.23 V and a substantial corrosion current density ($I_0 = 0.16$ A cm^{-2}), indicating significant metal degradation (Fig. 4a). The corrosion rate attains 1883 mm a^{-1}, indicating considerable deterioration in the acidic environment. In Na_2SO_4, the corrosion potential increases to −0.017 V, and the corrosion current significantly decreases to 4.3×10^{-6} A cm^{-2}, leading to a substantially reduced corrosion rate of 0.05 mm a^{-1}. These values indicate a stable passive film and reduced corrosion in a neutral environment, *i.e.*, a Na_2SO_4 electrolyte. Upon introducing the drug into the HCl solution, the E_0 values shifted to more positive values, and a decrease in I_0 was observed, indicating an inhibitory effect. At 50 ppm, the corrosion potential increases to 0.29 V, with I_0 around 4.5 μA cm^{-2} and a decreased corrosion rate of approximately 0.05 mm a^{-1}. Raising the concentration to 200 ppm further reduces the current density (2.8 μA cm^{-2}) and corrosion rate (0.033 mm a^{-1}), revealing high surface protection. The highest inhibition was observed at a high drug concentration (400 ppm), where the corrosion current decreased to 1.08 μA cm^{-2}, and the corrosion rate declined to 0.013 mm a^{-1}, indicating efficient adsorption of the drug molecules on the steel surface, resulting in a durable protective barrier. The EPR curves further validate this pattern (Fig. 4b). The charge linked to reactivation decreases with increasing drug concentration, from 0.009 C cm^{-2} in HCl to 0.0004 C cm^{-2} at 400 ppm, indicating reduced reactivation of the chromium-depleted zone and enhanced passivity. The polarization resistance (R_p) values increase significantly, from approximately 30 Ω cm^2 in HCl to around 64 000 Ω cm^2 at 400 ppm, indicating improved corrosion resistance. The PD and EPR analyses combined suggest that the examined medication functions as an effective mixed-type inhibitor, decreasing both anodic dissolution. The inhibitory efficacy increases with drug

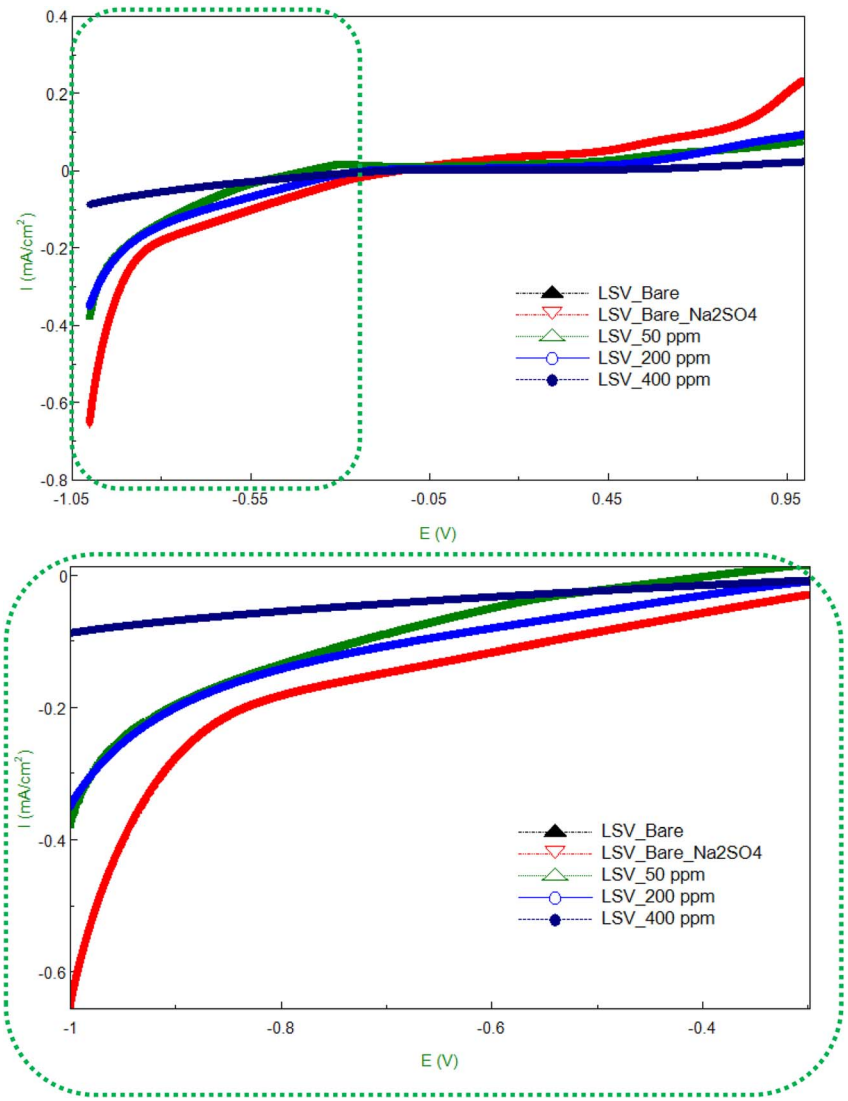

Fig. 6 LSV curves for 304 SS in different conditions.

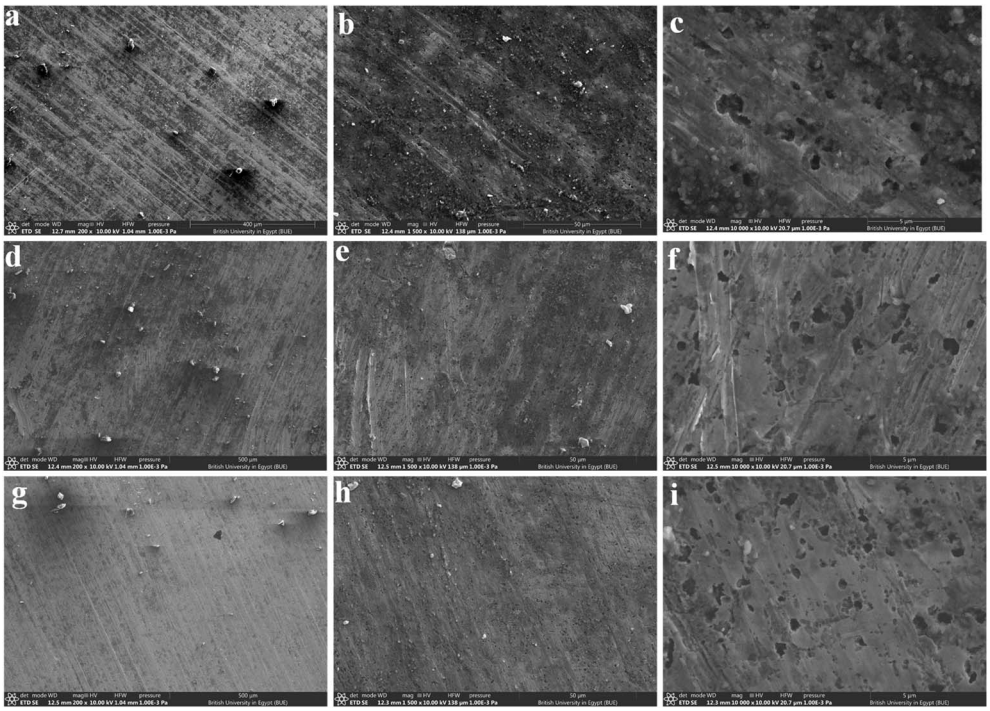

Fig. 7 SEM images of (a–c) pristine 304 SS, (d–i) 304 SS after treatment with (d–f) 50 ppm and (g–i) 400 ppm.

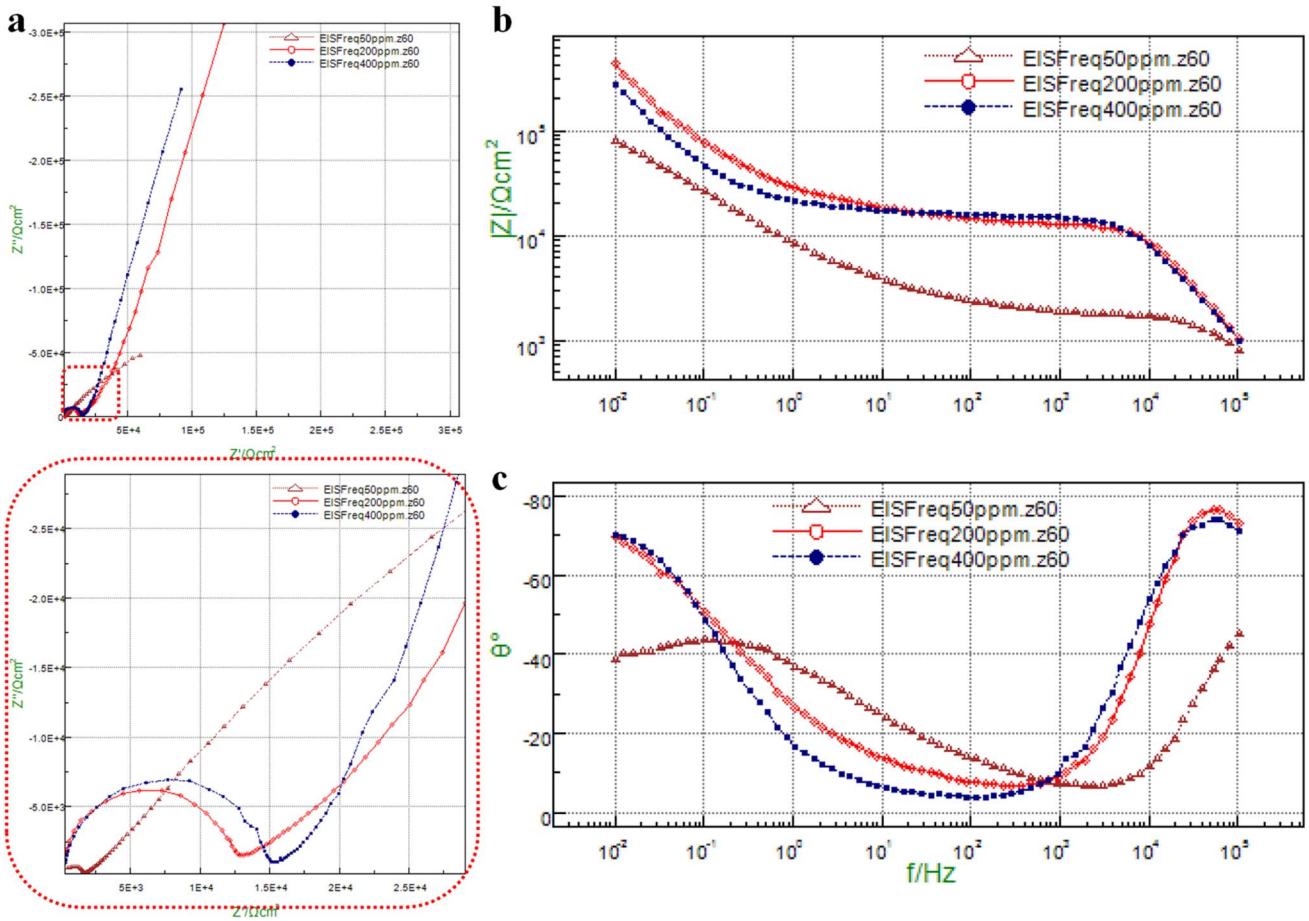

Fig. 8 EIS analysis (a) Nyquist plots, and (b and c) Bode plots.

concentration, primarily due to the adsorption of active functional groups (such as hydroxyl and amide) onto the steel surface, which obstructs aggressive chloride ion attack and fortifies the passive layer.

Fig. 5 enhances the PD/EPR findings by illustrating the system's behavior under time-resolved settings. In the chronopotentiometry (CP), the recorded steady potentials transition from highly active to progressively noble levels as the environment alters: HCl: −0.25 V, Na_2SO_4: +1.30 V, and HCl combined with the medication at concentrations of 50, 200, and 400 ppm yield +1.47, +1.62, and +2.12 V, respectively (Fig. 5a). The high negative potential in unadulterated HCl indicates a surface undergoing active corrosion, with the passive coating compromised and dissolution prevailing. Conversely, potential in a noncorrosive environment (*i.e.*, Na_2SO_4), particularly at high inhibitor concentrations, suggests the development or reinforcement of a passive/adsorbed protective layer. The consistent positive correlation with concentration indicates a distinct, dose-dependent enhancement in surface thermodynamic stability induced by the inhibitor. Fig. 5b (chronoamperometry, CA) offers kinetic validation. The current exhibits significant fluctuations in HCl, indicating continuous metal dissolution, film degradation, and potential localized phenomena (pitting) that result in temporary surges in anodic current. Conversely, the systems containing Na_2SO_4 and the administered drug demonstrate steady currents, with values indicative of the overall electrochemical activity: Na_2SO_4 of +1.27 μA cm^{-2}, HCl + 50 ppm ≈ +1.92 μA cm^{-2}, HCl + 200 ppm ≈ +0.57 μA cm^{-2}, and HCl + 400 ppm ≈ −0.31 μA cm^{-2}. The high variations in current for HCl indicate unregulated anodic dissolution. At a low drug inhibitor concentration (50 ppm), the current remains positive and exceeds that in Na_2SO_4, indicating incomplete surface covering and persistent anodic processes. Raising the concentration to 200 ppm significantly reduces the anodic current, thereby lowering dissolution rates and enhancing film coverage. At 400 ppm, the minor negative steady current indicates that cathodic processes marginally prevail, suggesting a net cathodic current, consistent with a well-formed protective layer inhibiting metal oxidation. The potentiostatic and amperometric time traces collectively demonstrate consistent and complementary behavior: the inhibitor functions in a concentration-dependent manner to (i) shift the metal to more noble potentials (stabilizing the surface) and (ii) decrease and ultimately reverse the net current, indicating significant suppression of anodic dissolution. The attenuation of current fluctuations at high drug concentrations suggests that the coating is both protective and mechanically and electrochemically stable under the specified conditions. These chrono-results therefore validate the PD/EPR findings that the medication offers high corrosion inhibition at adequate concentrations.

Fig. 6 presents LSV curves for 304 stainless steel in HCl, Na_2SO_4, and HCl containing different concentrations of the drug inhibitor (50, 200, and 400 ppm). The LSV technique provides insight into the system's anodic and cathodic polarization behavior, revealing how the applied potential affects corrosion and passivation. In the blank HCl solution (black curve), the current density increases sharply with potential,

Table 1 Potentiodynamic data fitting

	Tafel fitting					Tafel (LEV)					Integration		R_p fitting				
	β_a (mV)	β_c (mV)	I_0 (A cm^{-2})	E_0 (V)	Corrosion rate (mm a^{-1})	Residual	β_a (mV)	β_c (mV)	I_0 (A cm^{-2})	E_0 (V)	Corrosion rate (mm a^{-1})	Residual	Charge (Coul per cm^2)	R_p (Ω cm^2)	I_0 (μA cm^{-2})	E_0 (V)	Corrosion rate (mm a^{-1})	Inhibition efficiency (%)
HCl	20 940	27 631	0.16	−0.23	1883	0.0015	−620	209	0.0001	−0.24	13.1	0.009	0.21144	30	80	−0.234	10.1	0
Na_2SO_4	437	275	0.0000043	−0.017	0.05	1.7×10^{-7}	445	285	0.0000045	−0.02	0.053	8.7×10^{-11}	−0.0004	16 859	1.54	−0.016	0.018	99.9
50 ppm drug	764	417	0.0000045	0.288	0.053	2.82×10^{-7}	−22170	8653	0.0000049	0.29	0.058	1.89×10^{-8}	−0.0003	25 425	1.02	0.289	0.012	99.9
200 ppm	966	598	0.0000282	0.14	0.033	1.26×10^{-13}	22 170	8653	0.0000002	0.138	3.4×10^{-5}	7.8×10^{-9}	−0.00005	56 743	45	0.14	0.0054	99.9
400 ppm	2915	177	0.0000108	−0.065	0.013	1.88×10^{-7}	2072	181	0.0000093	−0.065	0.0108	1.89×10^{-10}	−0.0004	64 168	40.5	0.064	0.0047	99.9

reflecting active dissolution of the stainless steel surface due to aggressive chloride attack, leading to a high corrosion rate. This behavior indicates the absence of a stable passive film and continuous breakdown of the protective oxide layer. In contrast, the Na_2SO_4 environment shows a significantly lower current response over the potential range, suggesting that sulfate ions are more aggressive than chloride ions and can even help stabilize the passive oxide layer on stainless steel. Upon introducing the drug inhibitor, notable suppression in current density is observed, particularly at higher inhibitor concentrations. At 50 ppm, the current is slightly lower than that on bare steel in HCl, indicating partial adsorption of inhibitor molecules on the metal surface. The reduction is higher at 200 ppm, suggesting that the drug molecules effectively inhibit and partially block active sites. At 400 ppm, the current density is low and nearly constant over the potential range, demonstrating strong passivation and a highly protective film that effectively suppresses corrosion. The progressive reduction in current with increasing inhibitor concentration clearly reflects the drug's dose-dependent corrosion-inhibition behavior. The inhibitor likely adsorbs to the steel surface *via* heteroatoms (O, N) and π-electron interactions, forming a compact barrier that limits charge transfer. Thus, the LSV data confirm that the drug significantly enhances the corrosion resistance of 304 stainless steel in acidic chloride environments, with the best inhibition efficiency observed at 400 ppm. Table 1 shows coverage and inhibition corrosion of > 0.99% and >99.9%, respectively.

Mechanisms for inhibition

Organic corrosion inhibitors are a popular choice for protecting metal materials due to their high efficiency, reasonable cost, and strong feasibility. They can resist the intrusion of corrosive media by forming a protective film on the metal surface through electrostatic interactions (physical adsorption) or coordination bonds. They can be adsorbed to the surface of 304 SS, thereby effectively inhibiting the initiation and progression of pitting corrosion. The efficacy of an organic inhibitor is mainly ascribed to π bonds and/or extremely electronegative atoms or molecules that can donate electrons to impede the oxidation of the metal. Further analysis was performed using SEM images (Fig. 7) and EIS (Fig. 8). A scheme of the inhibition mechanism was presented in Fig. 9. The adsorption of expired drug molecules on the steel surface promotes surface passivation by maintaining the passive coating, decreasing metal dissolution (Fig. 9). The inhibitor molecules likely impede chloride-induced depassivation by blocking active sites and maintaining a more uniform electrochemical environment, thereby indirectly enhancing the stability of the austenitic phase.

Fig. 7 displays SEM micrographs of 304 SS surfaces under various conditions. Fig. 7a and b illustrate the unaltered 304 SS surface, which shows a heterogeneous morphology with many pores and surface imperfections measuring approximately 0.1–2.6 μm. These characteristics suggest surface imperfections that may serve as preferred sites for the initiation of localized corrosion in chloride-laden environments. After administering the expired drug inhibitor at a dose of 50 ppm (Fig. 7d–f), a significant decrease in both pore density and pore size is seen. The maximal pore size decreases to approximately 1.05 μm, indicating partial surface coverage by the inhibitor molecules and the initiation of protective film formation. The adsorbed layer effectively masks surface imperfections and prevents direct electrolyte contact with the steel substrate. At a high inhibitor concentration of 400 ppm (Fig. 7g–i), the surface morphology exhibits a notable increase in smoothness, accompanied by a further decrease in pore size to roughly 0.75 μm. Furthermore, the surface is progressively covered by a uniform white layer of adsorbed drug molecules. The layer's thickness and homogeneity increase with increasing inhibitor concentration, indicating improved adsorption and superior surface passivation. The SEM images reveal that a high inhibitor concentration improves surface coverage, reduces surface porosity, and strengthens the protective barrier against chloride-induced corrosion. The morphological alterations

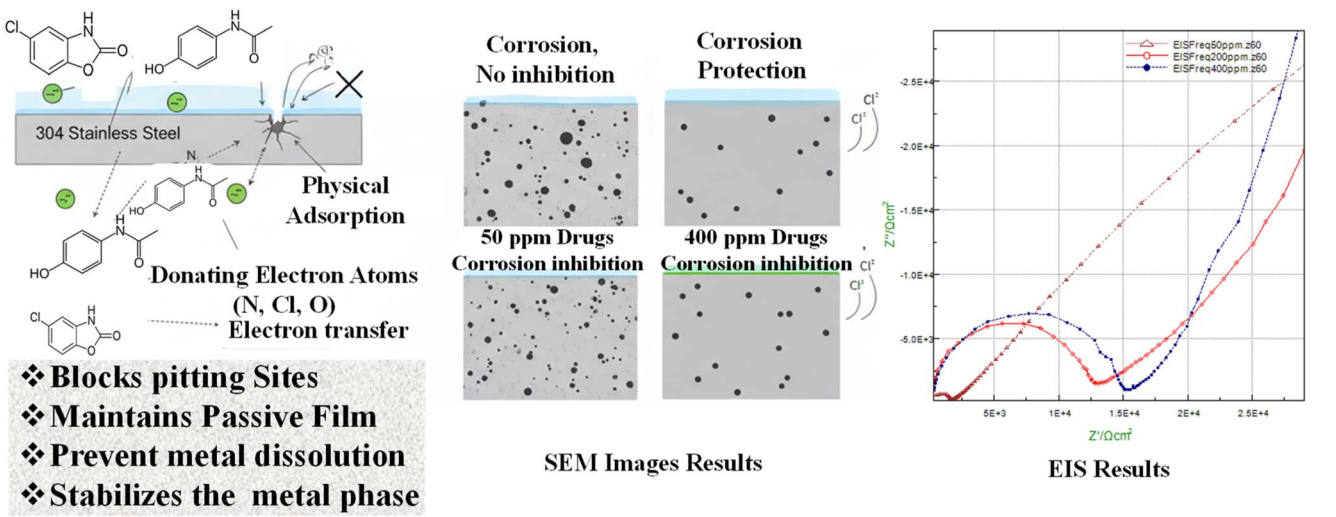

Fig. 9 Mechanism of corrosion inhibition on 304 stainless steel by adsorption of expired drug molecules.

Table 2 Summary for drugs reported as inhibitors for different steel

Inhibits	Substrate	Medium	Corrosion efficiency (%)	Inhibitor concentration (ppm)	Surface coverage	Ref.
Doxofylline	Soft steel	1 M HCl	72.84	200	0.7284	49
Dexamethasone sodium phosphate	Nitinol	PBS	31%		0.31	50
Lircetam	Low-carbon steel (LCS)	1 M HCl	98.16	60	0.9816	51
Fluimucil	Bronze	3.5 wt% NaCl	90.2	100	0.902	52
HBHC	A179 mild steel	1 M HCl	97.64	200	0.9764	53
Benzothiazolium salts	Carbon steel	1 M HCl	98.6	10^{-3} M	0.986	54
Chlorzoxazone (CHZ)	Mild steel (MS)	1 M HCl	88.3	1.0 ppm	0.883	55
Chlorzoxazone/*N*-acetyl-*para*-aminophenol	304 SS	1 M HCl	>99	200 ppm	0.99	This study

align with the electrochemical findings, indicating enhanced corrosion inhibition efficacy at elevated medication doses.

Fig. 8 illustrates the EIS results for 304 stainless steel in the presence of varying amounts of the expired drug inhibitor. Fig. 8a displays the Nyquist plots, which show that all spectra exhibit a single semicircle, indicative of charge-transfer-controlled corrosion at the metal/solution interface. The semicircle diameter steadily increases with drug loading, indicating a substantial increase in charge-transfer resistance (R_{ct}). This behavior suggests improved surface protection resulting from the adsorption of inhibitor molecules, which obstructs electron transport between the steel surface and the corrosive environment. Fig. 8b illustrates the associated Bode charts. The impedance modulus $|Z|$ at low frequencies rises with inhibitor concentration, further substantiating enhanced corrosion resistance. Furthermore, the phase angle widens and shifts to higher values as drug loading increases, indicating the formation of a more capacitive, uniform protective film on the 304 SS surface. The high phase angle signifies less surface heterogeneity and improved stability of the passive layer. The expansion of the Nyquist semicircle and the enhanced Bode characteristics at high inhibitor concentration indicate that the expired medication effectively mitigates corrosion by forming an adsorbed barrier layer that improves charge transfer resistance and surface passivation. The EIS results align well with the polarization and surface morphology investigations.

Pharmaceutical compounds have been widely investigated as corrosion inhibitors, with most reported drugs achieving inhibition efficiencies (IE%) above 90% due to their molecular structures containing π-bonds, aromatic rings, and heteroatom-based functional groups (–NH_2, –OH, –CN, –Cl) that enhance electron donation and adsorption onto metal surfaces (Table 2).[46–48] For example, expired doxofylline (DF) exhibited 72.84% IE at 200 ppm for soft steel in 1 M HCl, which increased to 88.48% upon addition of 50 ppm KI; surface roughness decreased from 606 nm to 294 nm, confirming the formation of a protective film through mixed-type inhibition.[49] Incorporation of dexamethasone sodium phosphate into LDH-coated NiTi alloys increased the interlayer spacing from 7.14 Å to 20.130 Å, improved corrosion resistance, and reduced drug release by 5%, demonstrating enhanced surface protection and biocompatibility.[50] Expired Lircetam (LRTM) showed excellent performance for low-carbon steel in 1 M HCl, achieving 98.16% IE at 60 ppm, following Langmuir adsorption behavior and mixed-type inhibition, as confirmed by electrochemical, SEM/AFM, and theoretical (DFT/MD) analyses.[51] Similarly, expired fluimucil (*N*-acetylcysteine) achieved an inhibition efficiency of 86.7% at 3.5 wt% NaCl and 90.2% in simulated acid rain, acting mainly as a cathodic inhibitor through Langmuir adsorption involving combined physisorption and chemisorption mechanisms (Table 2).[52] (*E*)-2-((2-hydroxybenzylidene))hydrazine-1-carboxamide (HBHC) demonstrated 94.50% (PP) and 93.33% (EIS) inhibition efficiencies at 200 ppm, maintaining 97.64% efficiency after 30 days, with theoretical calculations confirming strong adsorption *via* donor–acceptor interactions.[53] Benzothiazolium salts (BBEI and BCEI) achieved maximum efficiencies of 98.6% and 96.9%, respectively, at 10^{-3} M and 303 K in 1 M HCl, forming stable monolayer films consistent with Langmuir adsorption and mixed-type inhibition behavior.[54] A study investigated expired chlorzoxazone (CHZ) as a corrosion inhibitor for mild steel in 1.0 M HCl over 303–333 K using weight loss, electrochemical, surface characterization, and DFT analyses.[55] The results demonstrate that CHZ acts as a mixed-type inhibitor following Langmuir adsorption behavior, predominantly through physisorption, achieving up to 88.3% inhibition efficiency at 1.0 ppm by forming a protective hydrophobic adsorbed layer on the steel surface.[55] In comparison, chlorzoxazone/*N*-acetyl-*para*-aminophenol exhibited exceptionally high inhibition efficiency, exceeding 99.9% at only 200 ppm, highlighting their superior performance among reported pharmaceutical-based corrosion inhibitors (Table 2).

Conclusion

Electrochemical tests revealed that 304 stainless steel exhibits significant corrosion in 1.0 M HCl, characterized by a high corrosion current density (i_{corr}) and low polarization resistance (R_p), due to aggressive adsorption and infiltration of chloride ions. Conversely, exposure to Na_2SO_4 solution (noncorrosive, negative control experiment) yielded markedly reduced i_corr values and high R_p, substantiating the relatively less aggressive characteristics of sulfate ions. The incorporation of the expired medication

significantly enhanced corrosion resistance. At an optimum concentration of 400 ppm, the corrosion current density decreased by over an order of magnitude compared to the unrestrained HCl solution, while polarization resistance increased correspondingly, indicating an inhibition efficiency exceeding 99.9%. The OCP profiles exhibited consistent and less negative steady-state potentials over time, validating the development of a durable protective layer. Of the quantities examined (100–400 ppm), 400 ppm had the greatest inhibitory efficacy, correlating with nearly complete surface coverage ($\theta > 0.99$). These values indicate the development of a dense, adherent adsorbed coating that efficiently inhibited charge-transfer reactions at the metal/electrolyte interface. Electrochemical measurements corroborated these findings, indicating a significant decrease in anodic peak current density and inhibited active dissolution at elevated inhibitor doses. EIS revealed a notable increase in charge-transfer resistance (R_{ct}) and a decrease in double-layer capacitance, indicating inhibitor adsorption and decreased interfacial activity. The findings from PD, EPR, CA, CP, EIS, and SEM surface analysis substantiate that the expired medicine functions by adsorption onto the stainless steel surface. The inhibitor primarily acts as a mixed-type inhibitor, with anodic control predominating, markedly impeding metal dissolution. The pharmaceutical compound demonstrated significant inhibitory efficacy (>99% at 400 ppm), underscoring its promise as a cost-effective and environmentally sustainable corrosion inhibitor for 304 stainless steel in acidic conditions. Despite the expired pharmaceutical compound demonstrating exceptional corrosion-inhibition efficacy (>99% at 400 ppm) in laboratory settings, its long-term stability, effectiveness under industrial conditions and environmental implications necessitate additional research. Subsequent research should focus on mechanistic understanding through advanced surface characterisation and computational modelling, alongside scale-up assessment and comparison with commercial green inhibitors to confirm practical applicability.

Author contributions

Hani Nasser Abdelhamid: visualization, validation, supervision, software, resources, project administration, methodology, funding acquisition, investigation, formal analysis, data curation, conceptualization, writing – review & editing, writing – original draft. Mohamed Eissa, preparing drug solutions.

Conflicts of interest

The authors declare no competing interests.

Data availability

All raw data upon request from the corresponding author: Dr Abdelhamid.

Acknowledgements

This work was supported and funded by the Deanship of Scientific Research at Imam Mohammad Ibn Saud Islamic University (IMSIU) (grant number IMSIU-DDRSP2603).

References

1 A. Kumar, R. Sharma, S. Kumar and P. Verma, A Review on Machining Performance of AISI 304 Steel, *Mater. Today: Proc.*, 2022, **56**, 2945–2951, DOI: 10.1016/j.matpr.2021.11.003.
2 R. Kumar and A. K. Das, A Comprehensive Review of AISI 304 Steel Based on Different Thick Coating Process, *Mater. Today: Proc.*, 2024, **98**, 180–186, DOI: 10.1016/j.matpr.2023.10.080.
3 G. P. V. Dalmora, E. P. Borges Filho, A. A. Maraschin Conterato, W. S. Roso, C. E. Pereira and A. Dettmer, Methods of Corrosion Prevention for Steel in Marine Environments: A Review, *Results Surf. Interfaces*, 2025, **18**, 100430, DOI: 10.1016/j.rsurfi.2025.100430.
4 C. Q. Cheng, S. K. Yang and J. Zhao, Use of Color-Change Indicators to Quantify Passive Films on the Stainless Steel Valves of Nuclear Power Plants, *Nucl. Eng. Des.*, 2016, **297**, 267–275, DOI: 10.1016/j.nucengdes.2015.11.028.
5 M. Murmu, J. Heo, A. Alfantazi and S. O. Cho, Corrosion Inhibition of Stainless Steel through the Formation of Hydrophobic Nanoporous Oxide Layer, *Colloids Surf., A*, 2024, **697**, 134503, DOI: 10.1016/j.colsurfa.2024.134503.
6 Z. Zhang, J. Zhao, Y. Lei, Y. Wang, G. Zhou, C. Xu, Y. Rao and K. Wang, Preparation of Intricate Nanostructures on 304 Stainless Steel Surface by SiO2-Assisted HF Etching for High Superhydrophobicity, *Colloids Surf., A*, 2020, **586**, 124287, DOI: 10.1016/j.colsurfa.2019.124287.
7 W. Deng, R. Wang, S. Zhu, M. Hu, G. Chen, L. Wang and Y. Su, Eco-Friendly and Facile Method of Superhydrophobic Surface Fabricating on 304 Stainless Steel Substrates with Fluorine-Free Agents, *Surf. Coat. Technol.*, 2024, **478**, 130445, DOI: 10.1016/j.surfcoat.2024.130445.
8 D. G. Sacilotto, J. S. Costa and J. Z. Ferreira, Superhydrophobic Stearic Acid Deposited by Dip-Coating on AISI 304 Stainless Steel: Electrochemical Behavior in a Saline Solutions, *Mater. Res.*, 2022, **25**, DOI: 10.1590/1980-5373-mr-2022-0268.
9 H. Hu, X. Hong and Y. Gao, The Construction of Superhydrophobic Structure on Stainless Steel by an Optimized Chemical Etching Technics, *J. Eng. Mater. Technol.*, 2022, **144**, DOI: 10.1115/1.4051575.
10 M. Alonso Frank, A. R. Boccaccini and S. Virtanen, A Facile and Scalable Method to Produce Superhydrophic Stainless Steel Surface, *Appl. Surf. Sci.*, 2014, **311**, 753–757, DOI: 10.1016/j.apsusc.2014.05.152.
11 R. S. Almufarij, H. A. Fetouh El Sayed and M. E. Mohamed, Eco-Friendly Approach for the Construction of Superhydrophobic Coating on Stainless Steel Metal Based on Biological Metal–Organic Framework and Its Corrosion

Resistance Performance, *Materials*, 2023, **16**, 4728, DOI: 10.3390/ma16134728.

12 Y. Sun, D. Zhao and J. Song, Electrochemical Fabrication of Superhydrophobic 304 Stainless Steel by Neutral Electrolyte, *J. Mater. Sci.*, 2022, **57**, 20069–20081, DOI: 10.1007/s10853-022-07845-x.

13 D. Dwivedi, K. Lepková and T. Becker, Carbon Steel Corrosion: A Review of Key Surface Properties and Characterization Methods, *RSC Adv.*, 2017, **7**, 4580–4610, DOI: 10.1039/C6RA25094G.

14 J.-Y. Kim, I. Shin and J.-W. Byeon, Corrosion Inhibition of Mild Steel and 304 Stainless Steel in 1 M Hydrochloric Acid Solution by Tea Tree Extract and Its Main Constituents, *Materials*, 2021, **14**, 5016, DOI: 10.3390/ma14175016.

15 B. R. Holla, R. Mahesh, H. R. Manjunath and V. R. Anjanapura, Plant Extracts as Green Corrosion Inhibitors for Different Kinds of Steel: A Review, *Heliyon*, 2024, **10**, e33748, DOI: 10.1016/j.heliyon.2024.e33748.

16 J. Li, B. Lin, H. Zheng, Y. Wang, H. Zhang and J. Tang, The Effect of Elastic Tensile Stress on Inhibition Behavior of N-Lauroylsarcosine Sodium for 304L Stainless Steel Pitting Corrosion, *Corros. Sci.*, 2024, **233**, 112054, DOI: 10.1016/j.corsci.2024.112054.

17 X. Sun, L. He, P. Zhang and X. Zhang, Effect of Hydrocarbon Chain Length of Alkyl Trimethyl Ammonium Bromide on Corrosion Inhibition of Stainless Steel in Sulfuric Acid, *J. Solid State Electrochem.*, 2024, **28**, 3697–3711, DOI: 10.1007/s10008-024-05966-8.

18 A. A. Keshk, N. H. Elsayed, F. M. Almutairi, M. Al-Anazi, S. Said, H. M. Althurwi, R. K. Albalawi and M. R. El-Aassar, Effect of Green and Sustainable Extracted Fucoidan Polysaccharide as a Corrosion Inhibitor in 3.5% NaCl, *Biomass Convers. Biorefin.*, 2024, **14**, 28219–28232, DOI: 10.1007/s13399-022-03579-7.

19 B. G. P. Santos, A. A. Machado, M. S. Dias, T. A. Silva, A. da S. Neto, Â. Denadai and F. C. Oliveira, de Development of TiO2/Nb2O5 Films and Evaluation of Corrosion Prevention in AISI 304, *Steel Res. Int.*, 2024, **95**(6), 2300423, DOI: 10.1002/srin.202300423.

20 M. S. Dias, B. G. P. Santos, A. A. Machado, Â. M. L. Denadai, T. A. Silva, D. L. Rocco, M. de C. Santos, A. S. Neto and F. C. Oliveira, de Development, Characterization and Evaluation of TiO2/Nb5+ Thin Films with Potential for Corrosion Prevention of AISI 304 Steel in Acid Medium Containing Chloride Ions, *J. Mater. Sci.*, 2024, **59**, 12400–12417, DOI: 10.1007/s10853-024-09906-9.

21 T. Zuo, H. Guo, T. Yang, Y. Wei and M. Sun, WO3/In2S3 with NiOx for Photocathodic Protection of 304 Stainless Steel and for Inhibiting Sulfide Photocorrosion, *Mater. Lett.*, 2024, **377**, 137406, DOI: 10.1016/j.matlet.2024.137406.

22 N. Liu, L. Wang, X. Liu, Y. Lv, X. Zhu and C. Tang, Optimization on Microbial Anti-Scaling and Corrosion Inhibition Technology for Low Alkalinity and Low Hardness Circulating Cooling Water in Thermal Power Plants, *J. Phys.:Conf. Ser.*, 2024, **2731**, 012052, DOI: 10.1088/1742-6596/2731/1/012052.

23 Z. Li, Y. Ren, Z. Li, J. Zhang, Y. Fan, G. Jiang, D. Xu, T. Gu and F. Wang, Engineered Living Biofilm with Enhanced Metal Binding Ability for Corrosion Protection in Seawater, *Adv. Funct. Mater.*, 2024, **34**, 2313120, DOI: 10.1002/adfm.202313120.

24 K. A. Madurani, S. Firdausi, H. Harmami, I. Ulfin, E. Shinchi, S. R. Sari, M. Tominaga and F. Kurniawan, Improving Inhibition Efficiency of 304 Stainless Steel Using an Organic Extract in Acidic and High Temperature Environment: Experimental and Theoretical Studies, *Appl. Surf. Sci. Adv.*, 2024, **22**, 100620, DOI: 10.1016/j.apsadv.2024.100620.

25 F. Gapsari, P. H. Setyarini, F. Utaminingrum, A. M. Sulaiman, M. F. Haidar and T. S. Julian, Melaleuca Leaves Extract as Eco-Friendly Inhibitor for Low Carbon Steel in Sulfuric Acid, *Case Stud. Chem. Environ. Eng.*, 2024, **9**, 100657, DOI: 10.1016/j.cscee.2024.100657.

26 S. E. Hernández-Sánchez, J. P. Flores-De los Rios, H. A. Monreal-Romero, N. R. Flores-Holguin, L. M. Rodríguez-Valdez, M. Sánchez-Carrillo, A. D. Delgado and J. G. Chacón-Nava, Ruta Graveolens Plant Extract as a Green Corrosion Inhibitor for 304 SS in 1 M HCl: Experimental and Theoretical Studies, *Metals*, 2024, **14**, 1267, DOI: 10.3390/met14111267.

27 M. A. Deyab and Q. Mohsen, Protection of Stainless Steel Surfaces in Desalination Units against Corrosion during Acid Cleaning under Dynamic Conditions by Using Lavender Angustifolia Extract as a Green Inhibitor, *Sci. Rep.*, 2025, **15**, 4646, DOI: 10.1038/s41598-025-89206-7.

28 A. Sharma, J. Kaur and A. Saxena, Celastrus Paniculatus Seeds as a Green Corrosion Inhibitor for Stainless Steel in H2SO4 Acidic Solution, *J. Indian Chem. Soc.*, 2024, **101**, 101172, DOI: 10.1016/j.jics.2024.101172.

29 J. Li, D. Wang, X. Ouyang, Z. Tian, Y. Wu, B. Liu, Z. Li, E. Zhou, X. Li, F. Wang, *et al.*, Bifunctional Eco-Friendly Tobacco Stem Extract with Antibacterial and Corrosion Inhibition Properties for Mitigating Microbiologically Influenced Corrosion, *J. Mater. Sci. Technol.*, 2025, **257**, 46–59, DOI: 10.1016/j.jmst.2025.09.011.

30 B. A. Abd-El-Nabey, M. E. Mohamed, A. M. Helmy, H. Elnagar and A. M. Abdel-Gaber, Eco-Friendly Corrosion Inhibition of Steel in Acid Pickling Using Prunus Domestica Seeds and Okra Stems Extracts, *Int. J. Electrochem. Sci.*, 2024, **19**, 100695, DOI: 10.1016/j.ijoes.2024.100695.

31 E. K. Ardakani, E. Kowsari, A. Ehsani and S. Ramakrishna, Performance of All Ionic Liquids as the Eco-Friendly and Sustainable Compounds in Inhibiting Corrosion in Various Media: A Comprehensive Review, *Microchem. J.*, 2021, **165**, 106049, DOI: 10.1016/j.microc.2021.106049.

32 S. Hosny, A. Abdelfatah and G. A. Gaber, Synthesis, Characterization, Synergistic Inhibition, and Biological Evaluation of Novel Schiff Base on 304 Stainless Steel in Acid Solution, *Sci. Rep.*, 2024, **14**, 470, DOI: 10.1038/s41598-023-51044-w.

33 A. Elsamman, K. F. Khaled, S. A. Halim and N. S. Abdelshafi, A Critical View of the QSAR Model for the Prediction of a New Bispyrazole Derivative BPYR-P as a Corrosion Inhibitor for

304 SS in a 1.0 M HCl Solution, *J. Mol. Struct.*, 2024, **1297**, 136728, DOI: 10.1016/j.molstruc.2023.136728.

34 U. P. Kumar and B. He, Bin Synergistic Impact of Phytic Acid and Sodium Phosphate on the Corrosion Inhibition of Additively Manufactured 304L Steel in a 3.5 Wt% NaCl Medium, *J. Mater. Sci.*, 2025, **60**, 11092–11111, DOI: 10.1007/s10853-025-11085-0.

35 G. F. S. dos Santos, J. G. A. Rodrigues, S. B. Gomes Junior, T. M. N. da Silva, I. F. Schaffel, N. S. Conceição, G. R. Gonçalves, E. A. S. Filho and R. Q. Ferreira, From Waste to Protection: A Green Industrial Recycling Approach to Generate an Eco-Friendly Corrosion Inhibitor for 304 Stainless Steel in Saline Solutions, *J. Mater. Eng. Perform.*, 2025, **34**, 2703–2714, DOI: 10.1007/s11665-024-09318-5.

36 K. Haruna and T. A. Saleh, N-Vinylcaprolactam-Acrylamide Copolymer Inhibition Performance against 304L Stainless Steel Corrosion in a Simulated Sweet-Sour Corrosive Environment, *Mater. Today Commun.*, 2024, **40**, 109978, DOI: 10.1016/j.mtcomm.2024.109978.

37 A. A. Aguilar-Ruiz, R. G. Sánchez-Duarte, V. M. Orozco-Carmona, G. E. Devora-Isiordia, Y. Villegas-Peralta and J. Álvarez-Sánchez, Chitosan and Its Derivatives as a Barrier Anti-Corrosive Coating of 304 Stainless Steel against Corrosion in 3.5% Sodium Chloride Solution, *Coatings*, 2024, **14**, 1244, DOI: 10.3390/coatings14101244.

38 N. Hamad Al-Shaalan, G. A. Gaber, S. A. Mahmoud, S. Alharthi, A. Al-Naghmaish, M. Azizul Haque, M. Madani and M. Mohamady Ghobashy, Development and Performance Evaluation of Bio-Based Polymeric Composites as Multi-Environment Corrosion Inhibitors for Industrial Alloys, *Chem. Eng. Commun.*, 2025, 1–24, DOI: 10.1080/00986445.2025.2567874.

39 M. Abdallah, Rhodanine Azosulpha Drugs as Corrosion Inhibitors for Corrosion of 304 Stainless Steel in Hydrochloric Acid Solution, *Corros. Sci.*, 2002, **44**, 717–728, DOI: 10.1016/S0010-938X(01)00100-7.

40 W. El Mouhri, N. Tajat, W. El Hayaoui, I. Nadif, A. Idlahcen, S. Qourzal, I. Bakas, A. Legrouri, A. Assabbane, M. Badreddine, *et al.*, In Situ Growth of NiFe Layered Double Hydroxide Coating for the Corrosion Inhibition of 316 and 304 Stainless Steels in 3.5 Wt.% NaCl Solution, *J. Mater. Eng. Perform.*, 2025, **34**, 14467–14476, DOI: 10.1007/s11665-024-10169-3.

41 A. Veysi, M. Roushani and H. Najafi, Synthesis and Evaluation of CuNi-MOF as a Corrosion Inhibitor of AISI 304 and 316 Stainless Steel in 1N HCl Solution, *Heliyon*, 2025, **11**, e41296, DOI: 10.1016/j.heliyon.2024.e41296.

42 S. Mandal, D. Banik, P. K. Pandey, R. K. Gupta and K. Mondal, The Effect of Cattle Manure Extract on the Corrosion of SS304 in Different Aqueous Corrosives, *Bioresour. Technol. Rep.*, 2025, **30**, 102140, DOI: 10.1016/j.biteb.2025.102140.

43 M. A. Lawal, A. Musa, Z. Muhammad, K. Haruna and T. A. Saleh, Assessment of Inhibition Performance of Expired Chloroquine Phosphate on 304 L Stainless Steel Corrosion in Hydrochloric Acid Solution: An Experimental and Computational Study, *Sustainable Chem. Environ.*, 2025, **10**, 100251, DOI: 10.1016/j.scenv.2025.100251.

44 N. Anita, R. M. Joany, R. Dorothy, J. Aslam, S. Rajendran, A. Subramania, G. Singh, and C. Verma, Linear Polarization Resistance (LPR) Technique for Corrosion Measurements, in *Electrochemical and Analytical Techniques for Sustainable Corrosion Monitoring*, Elsevier, 2023, pp. 59–80.

45 A. Singh, K. R. Ansari, D. S. Chauhan, M. A. Quraishi, H. Lgaz and I.-M. Chung, Comprehensive Investigation of Steel Corrosion Inhibition at Macro/Micro Level by Ecofriendly Green Corrosion Inhibitor in 15% HCl Medium, *J. Colloid Interface Sci.*, 2020, **560**, 225–236, DOI: 10.1016/j.jcis.2019.10.040.

46 N. Vaszilcsin, A. Kellenberger, M. L. Dan, D. A. Duca and V. L. Ordodi, Efficiency of Expired Drugs Used as Corrosion Inhibitors: A Review, *Materials*, 2023, **16**, 5555, DOI: 10.3390/ma16165555.

47 N. Kumar, P. Anunay, S. Kumar, L. K. Meena and D. Singh, An Overview on Emerging Green Organic Corrosion Inhibitors: Sustainable Solution for Oil and Gas Industrial Applications, *RSC Adv.*, 2026, **16**, 3909–3948, DOI: 10.1039/D5RA08166A.

48 C. N. Njoku, B. N. Enendu, S. J. Okechukwu, N. Igboko, S. O. Anyikwa, A. I. Ikeuba, I. B. Onyeachu, I.-I. N. Etim and D. I. Njoku, Review on Anti-Corrosion Properties of Expired Antihypertensive Drugs as Benign Corrosion Inhibitors for Metallic Materials in Various Environments, *Results Eng.*, 2023, **18**, 101183, DOI: 10.1016/j.rineng.2023.101183.

49 A. G. Kalkhambkar, R. S K, J. Manjanna and G. H. Malimath, Effect of Expired Doxofylline Drug on Corrosion Protection of Soft Steel in 1 M HCl: Electrochemical, Quantum Chemical and Synergistic Effect Studies, *J. Indian Chem. Soc.*, 2022, **99**, 100639, DOI: 10.1016/j.jics.2022.100639.

50 M. Khakbiz, M. Chagami, S. Sheibani, E. Amiri, S. Moazzeni, S. Shakibania, Y. Hou and K.-B. Lee, Enhancement of Corrosion, Biocompatibility and Drug Delivery Properties of Nitinol Implants Surface by Al-Zn-LDH Nanohybrids, *Colloids Surf., A*, 2025, **704**, 135524, DOI: 10.1016/j.colsurfa.2024.135524.

51 S. D. Kotabagi, S. K. Rajappa, R. L. Minagalavar, M. R. Rathod, J. G. Suma and A. M. Sajjan, Expired Lircetam Drug as a Corrosion Inhibitor for Low-Carbon Steel in 1 M HCl: Experimental, Theoretical, and Quantum Chemical Insights, *Results Surf. Interfaces*, 2025, **18**, 100459, DOI: 10.1016/j.rsurfi.2025.100459.

52 S. Varvara, Reusing an Expired Drug as a Sustainable Corrosion Inhibitor for Bronze in 3.5% NaCl and Simulated Acid Rain Solutions, *Appl. Sci.*, 2025, **15**, 6637, DOI: 10.3390/app15126637.

53 H. Boughazi, Y. Boudinar, S. Tlili, A. Djedouani and N. Naili, Electrochemical, Surface, DFT, and ADMET Insights into (E)-2-(2-Hydroxybenzylidene)Hydrazine-1-Carboxamide as a Corrosion Inhibitor, *RSC Adv.*, 2025, **15**, 38946–38968, DOI: 10.1039/D5RA05876G.

54 A. Barrahi, M. E. M. Mekhzoum, M. Benkaddour, M. El Faydy, B. Dikici, R. Bouhfid, A. A. Farag, I. Warad, F. Bentiss and A. Zarrouk, Elucidating the Adsorption Mechanism and Corrosion Inhibition Performance of Benzothiazolium Salts on Carbon Steel in Acidic Solution, *RSC Adv.*, 2025, **15**, 46218–46242, DOI: 10.1039/D5RA07709E.

55 J. C. Abbar, G. A. Swetha, R. Rangappa, D. Priyadarshini, Y. Patil, M. Megalamani, G. Nagaraju and J. R. Choudhuri, Unlocking the Corrosion Inhibition Potential of Expired Chlorzoxazone on Mild Steel in Acidic Media: A Synergistic Approach with Electrochemical, Surface and Computational Insights, *Mater. Today Commun.*, 2025, **45**, 112409, DOI: 10.1016/j.mtcomm.2025.112409.